Check for updates

RESEARCH ARTICLE

NANO · MICRO small
www.small-journal.com

Weak Spots in Semiconductor Nanoplatelets: From Isolated Defects Toward Directed Nanoscale Assemblies

Volodymyr Shamraienko, Rico Friedrich, Subakti Subakti, Axel Lubk, Arkady V. Krasheninnikov, and Alexander Eychmüller**

The chemical engineering of nanostructures with atomic-scale precision is a fundamental scientific challenge. Cation exchange reactions in nanoplatelets (NPLs) offer an attractive platform for this precision chemistry, as it is relatively simple to carry out, extremely versatile, and allows the production of heterogeneous nanostructures that cannot be produced by any other means. A major hindrance has, however, been the lack of knowledge of the "weak spots" of the platelets where the ionic exchange reaction is initiated to optimally control the process toward directed nanoscale assemblies. Here, mercury selenide formation in cadmium selenide NPLs is investigated. The study of $Cd_{(1-n)}Hg_nSe$ NPLs using scanning transmission electron microscopy (STEM) pinpoints at the corners (vertices) and edges of the NPLs as the exchanged sites. Comprehensive first principles density functional calculations of Hg substitution energies in a hierarchy of models of four monolayers (ML) CdSe NPL stabilized with acetate ligands unambiguously underscore that the energetically preferred exchange positions are platelet corners — in line with the experimental findings. The results thus not only explain in detail how the cation exchange process in 2D CdSe NPLs is kicked-off, but also establish an arena for future studies in 2D nanomaterials reaching far beyond these reactions.

1. Introduction

One of the most frequently used approaches to change the properties of colloidal nanocrystals and to expand their applications is the cation exchange (CE) reaction.[1–6] This method is particularly advantageous for the targeted production of such nanomaterials (including specific size and shape), which to date cannot be produced by direct colloidal methods and consequently have not yet been sufficiently studied or used in applications. Despite the large number of new materials obtained through CE reactions on nanoparticles (NPs), the understanding of the overall process remains a challenge.[7] The complexity of the process can hardly be underestimated, as numerous factors such as crystal phase transformations, thermodynamics, kinetics, and ligands on the surface of the NPs, to name but a few, play a role and influence each CE reaction differently. Since nano chemistry involves "mix and try" methods, predicting the reaction outcome and fully understanding the CE mechanism is an extraordinary endeavor. However, the ever-growing demand for new nanomaterials, especially with 1D quantum confinement, requires not only a better general understanding of these types of reactions but also a deeper insight into where exactly the reaction starts and how it can be controlled and modeled.

V. Shamraienko, A. Eychmüller
Physical Chemistry
TU Dresden
Zellescher Weg 19, 01069 Dresden, Germany
E-mail: alexander.eychmueller@tu-dresden.de
R. Friedrich
Theoretical Chemistry
TU Dresden
Bergstraße 66c, 01062 Dresden, Germany
E-mail: rico.friedrich@tu-dresden.de

The ORCID identification number(s) for the author(s) of this article can be found under https://doi.org/10.1002/smll.202411112

© 2024 The Author(s). Small published by Wiley-VCH GmbH. This is an open access article under the terms of the Creative Commons Attribution-NonCommercial-NoDerivs License, which permits use and distribution in any medium, provided the original work is properly cited, the use is non-commercial and no modifications or adaptations are made.

DOI: 10.1002/smll.202411112

R. Friedrich, A. V. Krasheninnikov
Institute of Ion Beam Physics and Materials Research
Helmholtz-Zentrum Dresden-Rossendorf
01328 Dresden, Germany
R. Friedrich
Center for Extreme Materials
Duke University
Durham, NC 27708, USA
S. Subakti, A. Lubk
Institute for Solid State and Materials Research (IFW) Dresden
01069 Dresden, Germany
A. Lubk
Institute of Solid State and Materials Physics
TU Dresden
01069 Dresden, Germany

2D zincblende CdSe NPLs are an attractive platform for the preparation of various metal chalcogenides via a cation exchange reaction, especially when this is the only currently available way to achieve precise thickness control over the resulting structure while maintaining the lateral dimensions.[8–10] Unique optical properties of colloidal 2D CdSe NPLs related to strong 1D quantum confinement have attracted lots of attention since the publication of a milestone paper by Joo et al. in 2006 and Ithurria et al. in 2008.[11,12] Subsequently, the modification of the photophysical properties of cadmium chalcogenide NPLs became a major research activity, leading, e.g., to the fabrication of CdX (X = S, Se, Te) NPLs of varying lateral dimensions, atomically precise thicknesses, and their core/shell and core/crown variants.[12–17] This and the incorporation of impurities acting as dopants, the formation of cadmium chalcogenide alloyed NPLs and the metallic functionalization of NPLs offered a large number of potential applications of this material family.[18–21] At the same time, the direct fabrication of near-infrared (NIR) active 2D materials with a precise control over the number of atomic layers aka thickness remains a challenge, resulting in many reports on CE procedures. Various synthetic conditions of CE reactions on cadmium-based zincblende NPLs enables the production of 2D NIR active lead and mercury chalcogenides, but only few efforts have been made to understand how this transformation works and where it starts. In the work of Galle et al. a successful exchange reaction leads to the preparation of 3–6 mL PbSe NPLs with remarkable optical properties.[22] The driving force of this reaction was explained by the introduction of oleyl amine (OlAm), which acts as a hard base and forms a stable complex with Cd^{2+} ions acting as a hard acid according to the principle of hard and soft acids and bases (HSAB).[22,23] The same principle explains that Pb ions act as a soft acid, form a less stable complex with OlAm, and are therefore accessible to CE in this system. Later, Salzman and coworkers invoked the same approach and showed that PbSe domains initially form at the edges of the particle and can later incorporate Pb cations from these sites into the NPLs, exchanging Cd and changing the crystal structure from the original CdSe zinc blende to a PbSe rock salt.[24] The simultaneous exchange of ligands and cations without the addition of amines also leads to the complete exchange of cations; an explanation for this process has yet to be found.[25] Izquierdo et al., Mitrofanov et al., and Dabard et al. successfully prepared various mercury chalcogenides that illustrate their outstanding research in the field of CE reactions through the same HSAB explanation.[26–28] Mitrofanov et al. even speculated that densely packed surface ligands may reduce the permeability of incoming Hg^{2+} cations so that CE predominates at the platelet edges, which should have lower ligand density and greater accessibility to incoming cations.[27]

The great interest in CdSe NPLs as a platform for the production of various materials requires a better understanding of the CE process. While mechanistic insights have been provided by atomistic simulations with pseudoligands,[29] in particular the starting point of these reactions has not yet been sufficiently explored. In this work, we study the preferred starting position of CE in CdSe NPLs by transmission electron microscopy (TEM) and ab initio density functional theory (DFT) calculations. To overcome the challenge to quantify small numbers of Hg atoms in several nanometer thin (and electron-beam-damage sensitive) NPLs we employ high-angle annular dark field (HAADF) scanning TEM (STEM) that has been used to detect single foreign atoms on 2D materials previously.[30,31] Herein, we exploit the (roughly) Z^2 dependency of the (Rutherford-like) cross-section for electrons scattered into high angles to quantify the amount of Hg atoms relative to the CdSe background. From these data we estimate the amount of guest cations incorporated into the system and their spatial distribution, which, in combination with the computed substitution energies at different locations of the stabilized NPLs, shows that the energetically preferred position is always at the platelet corner. Our studies and modelling provide a new avenue for understanding and predicting CE chemistry in 2D CdSe NPLs, and we believe they can be applied to various 2D nanomaterials in general.

2. Results and Discussion

A seeded-growth approach was used to generate 4 mL CdSe NPLs with well-defined edges and corners, in contrast to direct synthesis routes, which can result in NPLs with irregular shapes (Figure S1, Supporting Information). On the resulting rectangular NPLs, we performed the CE reaction published by Mitrofanov and coworkers with a very small amount of mercury (2–10 mol.% of the amount of Cd in NPLs) and observed the same changes in the solution colors and absorption properties (**Figure 1a**).

Medium resolution TEM imaging showed no conspicuous changes or damage in the structure of the NPLs (Figure 1b–e). HRTEM and HAADF-STEM analyses were then performed to gain further insight into the starting point of the CE.

HRTEM analysis reveals the presence of crystal defects such as grain boundaries that may be introduced by the relatively high beam electron dose when focusing on a small crystal area. Thus, darker spots in the NPLs (Figure 1f), do not necessarily represent mercury-exchanged particle corners, but can also be a result of varying diffraction conditions in the presence of defects. The HAADF-STEM analysis (Figure 1g), on the other hand, is relatively insensitive to such diffraction effects, so that a *Z*-contrast evaluation can be performed to estimate the amount and position of the exchanged species.

To detect the small number of Hg atoms (i.e., on the order of 1 atom per nm^2 at $n = 0.1$ Hg doping level) and probe their distribution across the NPLs, we therefore employ HAADF-STEM analysis. Here, only electrons scattered into high angles (60 mrad–300 mrad) in our case, are collected by the detector and the detected intensities correspond to Rutherford cross-sections of screened Coulomb potentials, i.e., $I - Z^{1.7}$ with the atomic number *Z*.[32] Consequently, HAADF-STEM is very sensitive to large *Z* differences, facilitating the probing of a few Hg atoms in CdSe NPLs with a higher signal-to-noise ratio than spectroscopic EDX techniques (i.e., STEM EDX), suffering from very small cross-sections of core-loss excitations.[33] In our quantitative analysis of the composition, we furthermore take into account the stoichiometry of the NPLs $Cd_{(1-n)}Hg_nSe$, assume a constant thickness and a minimal HAADF intensity I_{min} occurring at the center of the NPL, where presumably no Hg is present. Under these assumptions, the (background subtracted) HAADF

© 2024 The Author(s). Small published by Wiley-VCH GmbH

16136829, 2025, 5, Downloaded from https://onlinelibrary.wiley.com/doi/10.1002/smll.202411112 by Sächsische Landesbibliothek Staats- Und Universitätsbibliothek Dresden, Wiley Online Library on [07/02/2025]. See the Terms and Conditions (https://onlinelibrary.wiley.com/terms-and-conditions) on Wiley Online Library for rules of use; OA articles are governed by the applicable Creative Commons License

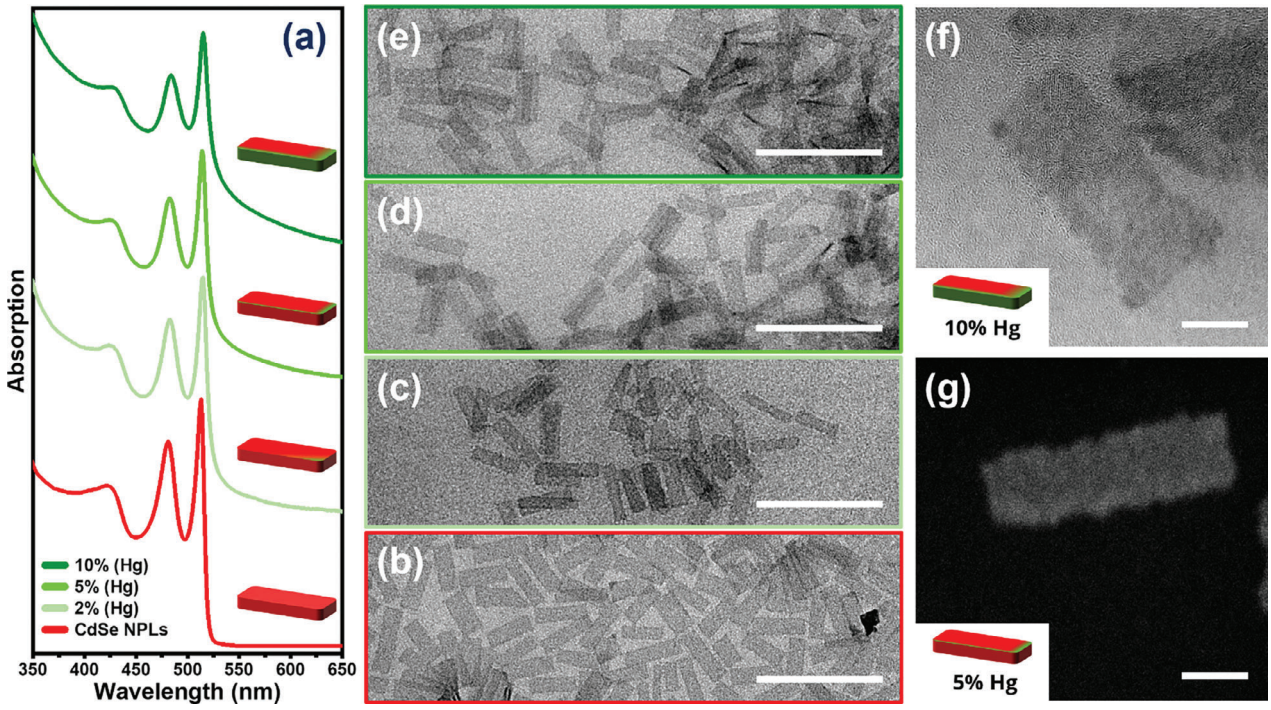

Figure 1. a) Absorption spectra of CdSe NPLs before and after the CE reaction with different amounts of guest cations (Hg). Corresponding medium-resolution TEM images (100 nm scalebar) of b) 4 mL CdSe NPLs before and after experimental CE with c) 2%, d) 5% and e) 10% Hg. f) HRTEM image (10 nm scalebar) of NPLs after CE aiming for 10% Cd/Hg exchange. g) HAADF-STEM image (10 nm scalebar) of NPLs after CE aiming for 5% Cd/Hg exchange.

intensity normalized with the minimal intensity can be expressed as ($Z_{Cd} = 48$, $Z_{Hg} = 80$, $Z_{Se} = 34$):

$$\frac{I\ (x,y)}{I_{min}} = \frac{(1 - n\ (x,y))\,48^{1.7} + n\,(x,y)\,80^{1.7} + 34^{1.7}}{80^{1.7} + 34^{1.7}} \quad (1)$$

Using this expression, we can estimate the mercury concentration in the following way:

$$n\ (x,y) = \left(\frac{I\ (x,y)}{I_{min}} - 1\right)\frac{48^{1.7} + 34^{1.7}}{80^{1.7} - 48^{1.7}} \quad (2)$$

As a sanity check, we always computed the average Hg content n and compare it to the nominal value (adjusted in the synthesis). **Figure 2** displays representative NPLs of $n = 0.1$ (Figure 2a), 0.05 (Figure 2b), 0.02 (Figure 2c) Hg doping, respectively.

The Hg profiles shown in Figure 2d were obtained by averaging over 5 NPLs, respectively (Figure S2–S4, Supporting Information). The profiles from NPLs with nominal $n \geq 0.05$ exhibit a characteristic increase of the Hg content toward the edges of the NPLs. The average doping determined from HAADF corresponds to $n = 0$, 0.06, 0.08, which agrees well with the nominal doping adjusted during synthesis, considering the low signal of

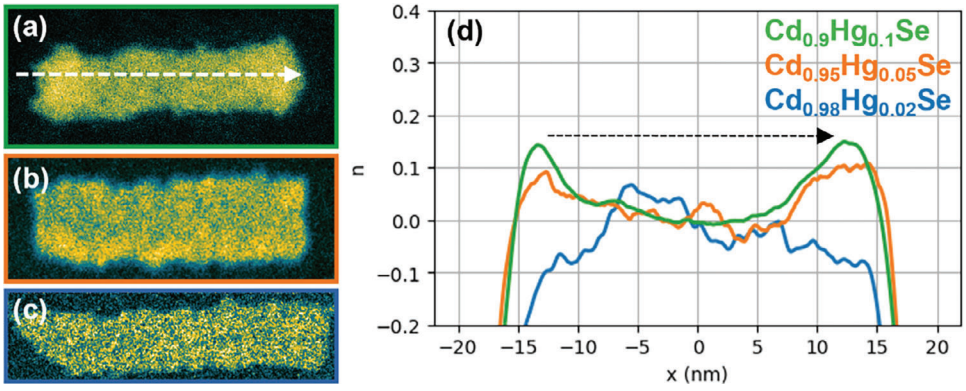

Figure 2. Hg composition analysis. HAADF STEM images of example CdSe NPLs after CE aiming for a) 10%, b) 5%, and c) 2% HAADF-STEM images reveal increased scattering cross-sections at particle edges and corners indicative of higher Hg content. The Hg content ***n*** in a small stripe along the NPL long axis extracted from an average over 5 NPLs reveals a systematic increase toward the edge. d) Note that negative concentration values toward the edges stem from violation of the constant thickness assumption used in the evaluation and are unphysical.

© 2024 The Author(s). Small published by Wiley-VCH GmbH

16136829, 2025, 5, Downloaded from https://onlinelibrary.wiley.com/doi/10.1002/smll.202411112 by Sächsische Landesbibliothek Staats- Und Universitätsbibliothek Dresden, Wiley Online Library on [07/02/2025]. See the Terms and Conditions (https://onlinelibrary.wiley.com/terms-and-conditions) on Wiley Online Library for rules of use; OA articles are governed by the applicable Creative Commons License

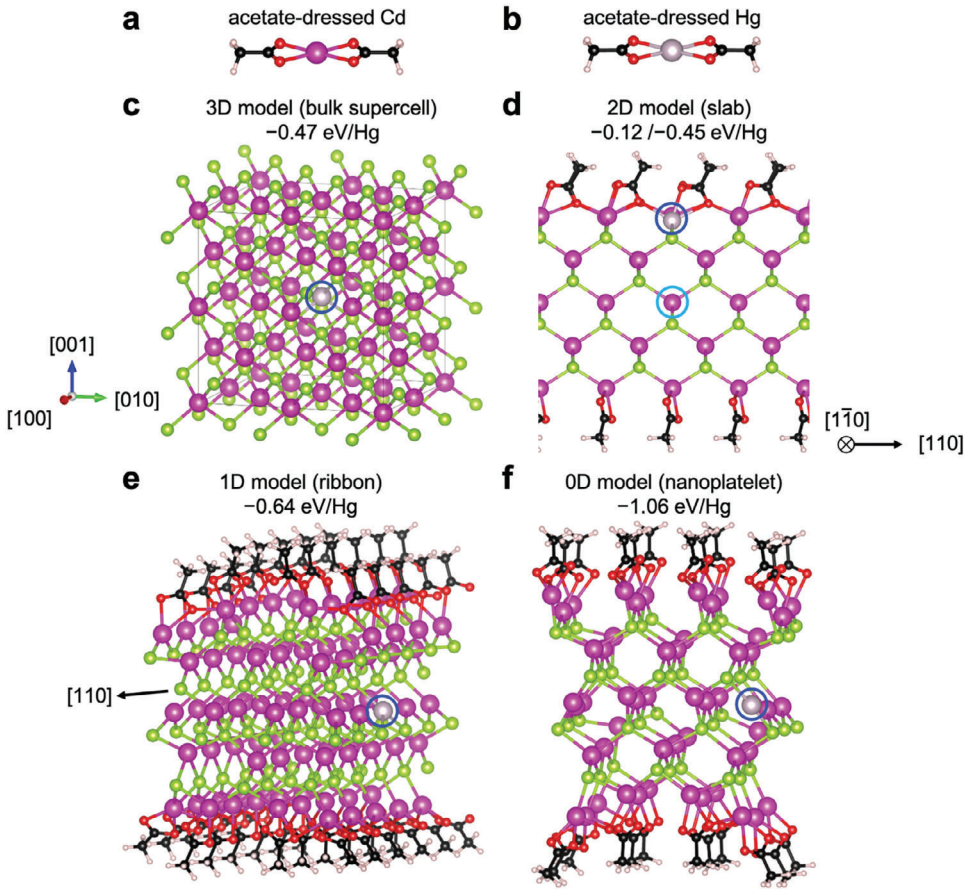

Figure 3. Cation exchange in a hierarchy of models with different dimensionality. The acetate-dressed cations of a) Cd and b) Hg. Hg substitution in c) a 3D model (bulk 2 × 2 × 2 supercell), d) a 2D model (slab with (001) surfaces), e) a 1D model (ribbon), and f) a 0D model (NPL). The respective substitution energies are also indicated. The substituting Hg ions are surrounded by a dark blue circle. In the case of the 2D slab, also the energy for substituting the central Cd marked by the light blue circle was calculated. Colors: Cd magenta, Se green, Hg gray, C black, O red, and H off-white.

a few Hg atoms and the noise and other artefacts in the HAADF-STEM data.

To gain atomistic insights into the Hg exchange energetics and to identify preferential exchange locations, we carried out comprehensive *ab initio* DFT calculations on a hierarchy of models with varying dimensionality (**Figure 3**). In each case, we compute the Hg exchange energy E_{ex} as the total energy difference between the final state (Hg impurity inside the respective CdSe system and separated Cd) and the initial state (pristine CdSe system and separated Hg):

$$E_{ex} = E\left(\mathrm{Hg@CdSe}\right) + E\left(\mathrm{Cd}\right) - \left(E\left(\mathrm{CdSe}\right) + E\left(\mathrm{Hg}\right)\right) \quad (3)$$

As the separated cation species Hg^{2+} and Cd^{2+} are not present in solution as free ions, they are modeled as "dressed" with ligands. To account for different reaction conditions, which effectively model different cation chemical potentials, two cases are distinguished: coverage by i) acetate and ii) methylamine. We thus focus on ligands with appropriate functional groups (amino and carboxyl) yet minimal length, as for instance full OlAm with its long side chain and many structural degrees of freedom cannot be modeled in large systems on an *ab initio* level. To obtain charge-neutral objects, two ligands are required in each case and the optimized structures of the acetate-dressed species are depicted in Figure 3a,b. We focus here on the acetate case and present an equivalent figure including the respective exchange energetics for methylamine dressing as Figure S5 (Supporting Information).

The first model for the exchange energetics is a 3D bulk 2 × 2 × 2 supercell (of the conventional CdSe cell) including a centrally placed Hg (Figure 3c). It is found that the reaction is only energetically favorable if the separated species are dressed with acetate leading to an energy gain of −0.47 eV whereas for the methylamine case, the corresponding value is +0.76 eV. The type of the ligand bound to the free species is thus crucial in determining the chemical potentials to obtain a favorable reaction. To further support this finding, we note that when the reaction energy is calculated assuming free atomic Hg/Cd in solution (since we expect charges to be strongly screened in this medium), the exchange energy is even higher, amounting to +1.43 eV.

To more closely match the actual NPL geometry in the experiment, a 2D slab model (with (001) surfaces) containing 5 Cd and 4 Se layers is considered in the next step (Figure 3d). Here, to maintain charge neutrality of the system, the top and bottom surfaces are covered with ligands and we note that our relaxed structure of the pristine slab closely resembles the one

 © 2024 The Author(s). Small published by Wiley-VCH GmbH

16136829, 2025, 5, Downloaded from https://onlinelibrary.wiley.com/doi/10.1002/smll.202411112 by Sächsische Landesbibliothek Staats- Und Universitätsbibliothek Dresden, Wiley Online Library on [07/02/2025]. See the Terms and Conditions (https://onlinelibrary.wiley.com/terms-and-conditions) on Wiley Online Library for rules of use; OA articles are governed by the applicable Creative Commons License

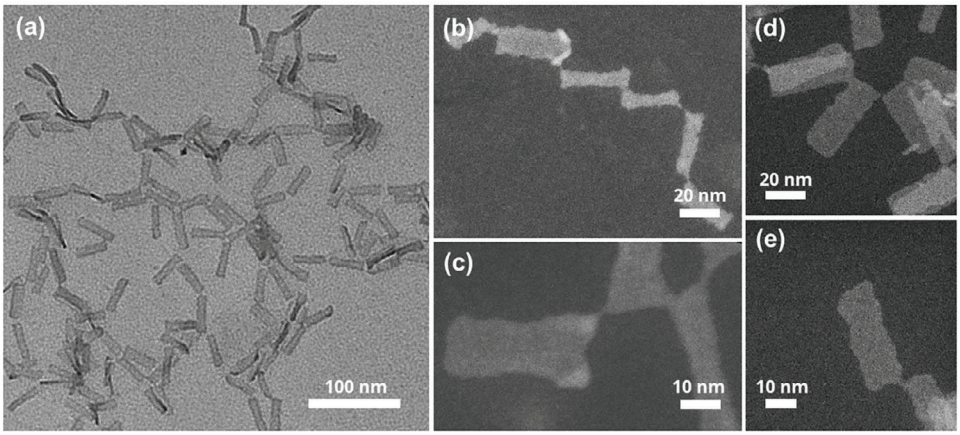

Figure 4. TEM analysis of NPLs after CE. a) TEM overview image of $Cd_{0.9}Hg_{0.1}Se$ NPLs. HAADF STEM of the b,c) $Cd_{0.9}Hg_{0.1}Se$, and d,e) $Cd_{0.95}Hg_{0.05}Se$ NPLs with different magnifications.

published by Koster et al.[34] The energy gain of Hg substitution is −0.12 eV (−0.45 eV) on the surface (within the center of the slab) for the acetate scenario in contrast to the methylamine case yielding +0.90 eV (+0.80 eV). Remarkably, the substitution thus releases less energy when taking place on the surface compared to within the slab which closely matches the energetics from the bulk as expected. As such, the ligand-covered surfaces are not likely a preferential spot for the (initial) exchange process.

On the next level, a 1D model (ribbon) of the same thickness as the slab and ≈1.3 nm width (7 CdSe units) is considered (Figure 3e). In order to maintain charge neutrality, again the top and bottom surfaces are ligand passivated but the ribbon edges remain uncovered. Now several different sites for Hg substitution relative to the edge and the top/bottom surfaces are available. An overview of the five different considered substitution sites and energy gains for both acetate and methylamine-covered ribbons are presented in Figure S6a,c (Supporting Information). Overall it is found that in both cases the sites directly at the ribbon edges as indicated in (Figure 3e) lead to the lowest exchange energy of −0.64 eV (+0.54 eV) for acetate (methylamine). This exceeds the above bulk substitution values and signifies that the ribbon edges are more preferential sites for the exchange than for instance the top and bottom surfaces.

Eventually, getting closest to the experimental conditions of a nanoscale geometry terminated in all three spatial directions, a 0D model (NPL) of ≈1.5 nm height (only considering the 5 Cd and 4 Se layers without ligands) as well as ≈1.3 and ≈1.0 nm width in each of the lateral directions is studied (Figure 3f). Guided again by charge neutrality considerations, the top and bottom surfaces are passivated by the ligands with all other edges uncovered. Also for this geometry, several different substitution sites at or close to the edges and corners of the platelet are available. The eight investigated sites and associated exchange energies for both ligand dressings are depicted in Figure S6b,d. The energetically most preferred spot with the highest energy gain for Hg substitution depicted in Figure 3f is an under-coordinated site right at the corner/vertex of the platelet with −1.06 eV (+0.17 eV) for acetate (methylamine). This site is not only most accessible and kinetic barriers are likely low, but also this highest energy gain among all considered substitution scenarios reveals it as the preferential location for the initiation of the cation exchange according to our computational modeling in agreement with the above experimental findings. To further validate the result, we also recomputed it to −1.08 eV by accounting for van der Waals interactions and applying dipole corrections for all structures involved corroborating that these effects play a minor role in the exchange energetics. The results thus consistently pinpoint at the platelet corners being the weak spots where the initial CE reaction takes place.

This understanding of the preferential reactive substitution sites at the atomic scale enables now engineering toward directed nanoscale assemblies. Further analysis of the NPLs after cation exchange showed that the weak spots can also be represented as binding sites between the particles. It can be clearly seen that the exchanged particles (**Figures** 4a and S3a,b) have orientated corner-to-corner binding sites. To better visualize these interconnection sites, we also performed HAADF-STEM analyses, which revealed that the particles grow into each other across the exchanged corners of the individual NPLs after both 10% (Figure 4b,c) and 5% (Figure 4d,e) exchange, creating a potential for directed alignment and the formation of a single-layer, corner-to-corner, interconnected superstructure based on semiconductor NPLs. We strongly believe that such superstructures will offer a versatile field of research for the creation of nanoscale arrays with targeted functionalities.

3. Conclusion

Employing the toolbox of CE reactions, we have successfully synthesized CdSe NPLs with targeted Hg concentrations ranging from 2 to ≈10%. The average doping determined from TEM agrees very well with the nominal doping adjusted during synthesis. Within the measurements, a characteristic increase of the Hg content toward the edges and corners of the NPLs is observed pointing toward preferential initial CE at these sites. To gain further understanding and atomistic insights into the energetics of the process, comprehensive *ab initio* DFT calculations were carried out. These firstly outline that dressing the free Hg and Cd species (in solution) with ligands is crucial to achieving the right chemical potential and thus correct energetics for the exchange

© 2024 The Author(s). Small published by Wiley-VCH GmbH

16136829, 2025, 5, Downloaded from https://onlinelibrary.wiley.com/doi/10.1002/smll.202411112 by Sächsische Landesbibliothek Staats- Und Universitätsbibliothek Dresden, Wiley Online Library on [07/02/2025]. See the Terms and Conditions (https://onlinelibrary.wiley.com/terms-and-conditions) on Wiley Online Library for rules of use; OA articles are governed by the applicable Creative Commons License

reaction. Only a dressing with acetate ligands leads to an energetic preference for the CE to take place. Based on investigating a hierarchy of models of different dimensionality, the most favorable exchange sites with the highest energy gain are undercoordinated sites at the corners of the NPLs coinciding with the electron microscopy findings. As such, our work not only clearly pinpoints the weak spots of the NPLs where the CE reaction is initiated, but it thereby also provides clear guidelines to optimize the exchange reaction and to design (coupled) 2D nanomaterials.

4. Experimental Section

All the NPLs discussed were prepared according to the synthesis published previously.[27]

The *ab initio* calculations were performed with AFLOW[35,36] and the Vienna ab-initio simulation package (VASP)[37–39] employing the PBE[40] functional with parameters in accordance with the AFLOW standard[41] as well as setting the internal VASP precision to ACCURATE. The relaxation of the NPLs was carried out with precision NORMAL and the default number of bands set by VASP. For the final relaxed structure as well as all platelet systems with Hg substitution, a static calculation with precision elevated again to ACCURATE was performed to compute the exchange energies.

The 2D (001) slabs were constructed from the bulk standard conventional unit cell with the respective AFLOW commands[42] resulting in structures containing 5 Cd and 4 Se layers according to experiment and including at least 12 Å of vacuum perpendicular to the surface. For the calculations with the Hg impurities, 3 × 3 in-plane supercells are used resulting in distances between periodic images of the mercury ions of at least 12 Å. The ribbon was constructed from the slab by generating a 2 × 1 in-plane supercell and removing all atoms except for the left 7 CdSe layers and ligands bound to the respective top and bottom surfaces. The resulting vacuum between ribbon edges in different cells amounted to ≈14 Å and atoms from ligands belonging to different ribbons were at least 10 Å away from each other in the relaxed geometries. The distance between different Hg along the ribbon edge was again at least 12 Å. The nano-platelet is constructed from a 1 × 2 supercell of the ribbon by removing the atoms of the upper half which resulted in a model containing a total of 264 atoms (54 Cd, 42 Se, 48 C, 48 O, and 72 H) and at least 10 Å of vacuum in all three spatial directions. For the slab, ribbon, and NPL, the Brillouin zone was sampled only at the Γ-point. For the slab and the ribbon, both the ionic coordinates as well as the cell shape were allowed to relax while keeping the cell volume constant to properly account for the relaxation of in-plane cell parameters. To economize computational resources, the structures with the Hg impurities were only relaxed in the case of the bulk supercell and the slab, while for the ribbon and NPL only a static electronic calculation was performed. This approximation was validated for the slab, where the relaxation only led to an energy gain of ≈0.16 eV per Hg which is significantly lower than the overall exchange energies.

As the CdSe systems with single Hg substitution were asymmetric and could thus create an electric dipole, the significance of dipole corrections to the energy, potential, and forces was investigated. It was found that the dipole corrections were small and largely cancelled when computing the energy difference between the pristine and substituted systems such that it only varied by a few meV upon inclusion of these corrections. Also when taking into account van der Waals interactions within the DFT-D3 approximation,[43] the Hg exchange energy was only modified by a few 10 meV as mentioned in the main text even when considering structural relaxation of the Hg impurity system.

The ligand-dressed cations (free Cd/Hg atoms) were modeled in a 25Å × 15Å × 15Å (15Å × 15Å × 15Å) cell using Γ-only *k*-point sampling and all structural degrees of freedom were relaxed until the total energy change dropped below 10^{-5} eV resulting in all force components being smaller than 20 meV $Å^{-1}$.

Overview images of NPLs were acquired employing phase contrast TEM (defocused) with and without additional contrast aperture. HAADF *Z*-contrast imaging was carried out at the probe corrected FEI Titan[3] 80–300 kV TEM employing an acceleration voltage of 300 kV. Bright-field electron microscopy was carried out on a JEOL JEM-1400Plus microscope operated at 120 kV.

Supporting Information

Supporting Information is available from the Wiley Online Library or from the author.

Acknowledgements

V.S. and R.F. contributed equally to this work. The authors thank Stefano Curtarolo for fruitful discussions. R.F. acknowledges funding from the German Research Foundation (DFG), project FR 4545/2-1, and for the "Autonomous Materials Thermodynamics" (AutoMaT) project by Technische Universität Dresden and Helmholtz-Zentrum Dresden-Rossendorf within the DRESDEN-concept alliance as well as support from the Alexander von Humboldt Foundation under the Feodor Lynen research fellowship. A.E., A.V.K., R.F., V.S., S.S, A.L. thank the DFG for the support through the collaborative research center "Chemistry of Synthetic 2D Materials" SFB-1415-417590517. The authors thank the HZDR Computing Center, HLRS Stuttgart (HAWK cluster), the Paderborn Center for Parallel Computing (PC2, Noctua 2 cluster), and TU Dresden ZIH (Taurus cluster) for generous grants of CPU time.

Open access funding enabled and organized by Projekt DEAL.

Conflict of Interest

The authors declare no conflict of interest.

Data Availability Statement

The data that support the findings of this study are available from the corresponding author upon reasonable request.

Keywords

cation exchange, DFT, HAADF STEM, nanoplatelets

Received: November 20, 2024
Published online: December 18, 2024

[1] D. Arora, S. Y. Tan, S. W. Tong, P. C. Lim, P. N. Suseela Nair, M. Lin, Q. Zhu, Q. Yan, W. Y. Wu, *ACS Appl. Nano Mater.* **2023**, *7*, 18189.
[2] J. M. Veglak, C. H. Jeong, H. L. Young, S. K. O'Boyle, R. E. Schaak, *ACS Mater. Lett.* **2023**, *5*, 3000.
[3] Y. Feng, Y. Ji, Y. Zhang, Q. Shao, Y. Xu, Y. Li, X. Huang, *Nat. Synth.* **2022**, *1*, 626.
[4] L. De Trizio, L. Manna, *Chem. Rev.* **2016**, *116*, 10852.
[5] Z. Li, M. Saruyama, T. Asaka, T. Teranishi, *Nat. Commun.* **2024**, *15*, 4899.
[6] Q. Zhang, K. Yin, H. Dong, Y. Zhou, X. Tan, K. Yu, X. Hu, T. Xu, C. Zhu, W. Xia, F. Xu, H. Zheng, L. Sun, *Nat. Commun.* **2017**, *8*, https://doi.org/10.1038/ncomms14889.
[7] S. S. Lee, P. Fenter, K. L. Nagy, N. C. Sturchio, *Nat. Commun.* **2017**, *8*, 15826.
[8] C. Bouet, D. Laufer, B. Mahler, B. Nadal, H. Heuclin, S. Pedetti, G. Patriarche, B. Dubertret, *Chem. Mater.* **2014**, *26*, 3002.

© 2024 The Author(s). Small published by Wiley-VCH GmbH

16136829, 2025, 5, Downloaded from https://onlinelibrary.wiley.com/doi/10.1002/smll.202411112 by Sächsische Landesbibliothek Staats- Und Universitätsbibliothek Dresden, Wiley Online Library on [07/02/2025]. See the Terms and Conditions (https://onlinelibrary.wiley.com/terms-and-conditions) on Wiley Online Library for rules of use; OA articles are governed by the applicable Creative Commons License

[9] N. Fu, H. Lehouelleur, L. Makké, L. Curti, C. Dabard, E. Bossavit, X. Z. Xu, D. Pierucci, M. G. Silly, G. Patriarche, E. Lhuillier, B. T. Diroll, S. Ithurria, *Chem. Mater.* **2024**, *36*, 5204.
[10] T. Galle, M. Kazes, R. Hübner, J. Lox, M. Samadi Khoshkhoo, L. Sonntag, R. Tietze, V. Sayevich, D. Oron, A. Koitzsch, V. Lesnyak, A. Eychmüller, *Chem. Mater.* **2019**, *31*, 5065.
[11] J. Joo, J. S. Son, S. G. Kwon, J. H. Yu, T. Hyeon, *J. Am. Chem. Soc.* **2006**, *128*, 5632.
[12] S. Ithurria, B. Dubertret, *J. Am. Chem. Soc.* **2008**, *130*, 16504.
[13] A. Prudnikau, A. Chuvilin, M. Artemyev, *J. Am. Chem. Soc.* **2013**, *135*, 14476.
[14] S. Pedetti, S. Ithurria, H. Heuclin, G. Patriarche, B. Dubertret, *J. Am. Chem. Soc.* **2014**, *136*, 16430.
[15] S. Pedetti, B. Nadal, E. Lhuillier, B. Mahler, C. Bouet, B. Abécassis, X. Xu, B. Dubertret, *Chem. Mater.* **2013**, *25*, 2455.
[16] S. Ithurria, M. D. Tessier, B. Mahler, R. P. S. M. Lobo, B. Dubertret, A. L. Efros, *Nat. Mater.* **2011**, *10*, 936.
[17] B. Mahler, B. Nadal, C. Bouet, G. Patriarche, B. Dubertret, *J. Am. Chem. Soc.* **2012**, *134*, 18591.
[18] M. Dufour, E. Izquierdo, C. Livache, B. Martinez, M. G. Silly, T. Pons, E. Lhuillier, C. Delerue, S. Ithurria, *ACS Appl. Mater. Interfaces* **2019**, *11*, 10128.
[19] A. Antanovich, L. Yang, S. C. Erwin, B. Martín-García, R. Hübner, C. Steinbach, D. Schwarz, N. Gaponik, V. Lesnyak, *Chem. Mater.* **2022**, *34*, 10361.
[20] B. Mahler, L. Guillemot, L. Bossard-Giannesini, S. Ithurria, D. Pierucci, A. Ouerghi, G. Patriarche, R. Benbalagh, E. Lacaze, F. Rochet, E. Lhuillier, *J. Phys. Chem. C* **2016**, *120*, 12351.
[21] A. H. Khan, V. Pinchetti, I. Tanghe, Z. Dang, B. Martín-García, Z. Hens, D. Van Thourhout, P. Geiregat, S. Brovelli, I. Moreels, *Chem. Mater.* **2019**, *31*, 1450.
[22] T. Galle, M. Samadi Khoshkhoo, B. Martin-Garcia, C. Meerbach, V. Sayevich, A. Koitzsch, V. Lesnyak, A. Eychmüller, *Chem. Mater.* **2019**, *31*, 3803.
[23] R. G. Pearson, *J. Chem. Educ.* **1968**, 581.
[24] B. B. V. Salzmann, J. de Wit, C. Li, D. Arenas-Esteban, S. Bals, A. Meijerink, D. Vanmaekelbergh, *J. Phys. Chem. C* **2022**, *126*, 1513.
[25] T. Galle, D. Spittel, N. Weiß, V. Shamraienko, H. Decker, M. Georgi, R. Hübner, N. Metzkow, C. Steinbach, D. Schwarz, V. Lesnyak, A. Eychmüller, *J. Phys. Chem. Lett.* **2021**, *12*, 5214.
[26] E. Izquierdo, M. Dufour, A. Chu, C. Livache, B. Martinez, D. Amelot, G. Patriarche, N. Lequeux, E. Lhuillier, S. Ithurria, *Chem. Mater.* **2018**, *30*, 4065.
[27] A. Mitrofanov, A. Prudnikau, F. Di Stasio, N. Weiß, R. Hübner, A. M. Dominic, K. B. L. Borchert, V. Lesnyak, A. Eychmüller, *Chem. Mater.* **2021**, *33*, 7693.
[28] C. Dabard, J. Planelles, H. Po, E. Izquierdo, L. Makke, C. Greboval, N. Moghaddam, A. Khalili, T. H. Dang, A. Chu, S. Pierini, C. Abadie, M. Cavallo, E. Bossavit, X. Z. Xu, P. Hollander, M. Silly, E. Lhuillier, J. I. Climente, S. Ithurria, *Chem. Mater.* **2021**, *33*, 9252.
[29] Z. Fan, L. C. Lin, W. Buijs, T. J. H. Vlugt, M. A. Van Huis, *Nat. Commun.* **2016**, *7*, 11503.
[30] J. Lee, W. Zhou, S. J. Pennycook, J. C. Idrobo, S. T. Pantelides, *Nat. Commun.* **2013**, *4*, 1650.
[31] J. C. Meyer, C. O. Girit, M. F. Crommie, A. Zettl, *Nature* **2008**, *454*, 319.
[32] P. D. Nellist, in *Scanning Transmission Electron Microscopy: Imaging and Analysis*, (Eds.: S. J. Pennycook, P. D. Nellist), Springer, New York **2011**, pp. 91–115.
[33] M. X.-R Watanabe., in *Scanning Transmission Electron Microscopy: Imaging and Analysis*, (Eds.: S. J. Pennycook, P. D. Nellist), Springer, New York **2011**, pp. 291–351.
[34] R. S. Koster, C. Fang, A. Van Blaaderen, M. Dijkstra, M. A. Van Huis, *Phys. Chem. Chem. Phys.* **2016**, *18*, 22021.
[35] C. Oses, M. Esters, D. Hicks, S. Divilov, H. Eckert, R. Friedrich, M. J. Mehl, A. Smolyanyuk, X. Campilongo, A. van de Walle, J. Schroers, A. G. Kusne, I. Takeuchi, E. Zurek, M. B. Nardelli, M. Fornari, Y. Lederer, O. Levy, C. Toher, S. Curtarolo, *Comput. Mater. Sci.* **2023**, *217*, 111889.
[36] M. Esters, C. Oses, S. Divilov, H. Eckert, R. Friedrich, D. Hicks, M. J. Mehl, F. Rose, A. Smolyanyuk, A. Calzolari, X. Campilongo, C. Toher, S. Curtarolo, *Comput. Mater. Sci.* **2023**, *216*, 1.
[37] G. Kresse, J. Hafner, *Phys. Rev. B* **1993**, *47*, 558.
[38] G. Kresse, J. Furthmüller, *Phys. Rev. B* **1996**, *54*, 11169.
[39] G. Kresse, J. Furthmüller, *Comput. Mater. Sci.* **1996**, *6*, 15.
[40] J. P. Perdew, K. Burke, M. Ernzerhof, *Phys. Rev. Lett.* **1996**, *77*, 3865.
[41] C. E. Calderon, J. J. Plata, C. Toher, C. Oses, O. Levy, M. Fornari, A. Natan, M. J. Mehl, G. Hart, M. Buongiorno Nardelli, S. Curtarolo, *Comput. Mater. Sci.* **2015**, *108*, 233.
[42] R. V. Chepulskii, S. Curtarolo, *Appl. Phys. Lett.* **2010**, *97*, 221908.
[43] S. Grimme, J. Antony, S. Ehrlich, H. Krieg, *J. Chem. Phys.* **2010**, *132*, 154104.

© 2024 The Author(s). Small published by Wiley-VCH GmbH

16136829, 2025, 5, Downloaded from https://onlinelibrary.wiley.com/doi/10.1002/smll.202411112 by Sächsische Landesbibliothek Staats- Und Universitätsbibliothek Dresden, Wiley Online Library on [07/02/2025]. See the Terms and Conditions (https://onlinelibrary.wiley.com/terms-and-conditions) on Wiley Online Library for rules of use; OA articles are governed by the applicable Creative Commons License